recycling

MDPI

Article

Extended Material Recovery from Municipal Solid Waste Incinerator Bottom Ash Using Magnetic, Eddy Current, and Density Separations

Ida Bagus Gede Sumbranang Adhiwiguna [1,*], Keshalinni Ramalingam [1], Karl-Heinz Becker [2], Alexander Khoury [2], Ragnar Warnecke [3] and Rüdiger Deike [1]

[1] Chair of Metallurgy—Institut für Technologien der Metalle, Universität Duisburg Essen, Friedrich-Ebert-Str. 12, 47119 Duisburg, Germany; ruediger.deike@uni-due.de (R.D.)
[2] STEINERT GmbH, Widdersdorferstr. 329-331, 50933 Köln, Germany
[3] GKS-Gemeinschaftskraftwerk Schweinfurt GmbH, Hafenstraße 30, 97424 Schweinfurt, Germany
* Correspondence: ida.adhiwiguna@uni-due.de or ida.adhiwiguna@gmail.com

Abstract: This research introduces an extended processing method for increasing the possibility of valorizing processed IBA (pr.IBA), which is currently only used as a construction material in landfill sites, considering its immense potential in valuable metal and mineral concentrations. Following a selective milling process, an extended material recovery sequence involving a magnetic, eddy current, and density separation sequence is developed. Based on the observations and outcomes explored in the present study, a substantially reliable and practical industrial approach is designed and tested to generate a cleaner mineral fraction and complementarily collect valuable metals from pr.IBA. Specifically, four enhanced valuable product streams can be anticipated, output mineral, high-magnetic, low-magnetic, and non-ferrous, which can be further utilized as alternative materials for cement clinker and concrete production coupled with iron, copper, and aluminum recovery in a conventional recycling operation. Therefore, in addition to introducing an additional perspective and moving one step closer to closing the waste management loop, this proposed method offers the opportunity to save primary materials and reduce carbon emissions by providing valuable alternative secondary resources.

Keywords: MSW incineration; bottom ash; magnetic; eddy current; separation; recycling

Academic Editors: Sossio Fabio Graziano, Rossana Bellopede, Giovanna Antonella Dino and Nicola Careddu

Received: 28 November 2024
Revised: 15 January 2025
Accepted: 17 January 2025
Published: 24 January 2025

Citation: Adhiwiguna, I.B.G.S.; Ramalingam, K.; Becker, K.-H.; Khoury, A.; Warnecke, R.; Deike, R. Extended Material Recovery from Municipal Solid Waste Incinerator Bottom Ash Using Magnetic, Eddy Current, and Density Separations. *Recycling* **2025**, *10*, 16. https://doi.org/10.3390/recycling10010016

1. Introduction

Waste-to-energy (WtE) plants have long been recognized as one of the reliable alternatives for waste management and promoting a circular economy through the valorization of municipal solid waste (MSW) [1–3]. However, the complete elimination of MSW through incineration is rarely achieved, as it depends on the composition of the input material. One of the primary residues is incinerator bottom ash (IBA), which constitutes ca. 25% of the total input MSW and is considered a low-value material as it is only utilized limitedly in landfill construction. Considering the case in Germany, according to a survey conducted in 2021 by the German Association of WtE Plants (ITAD) and the Association of IBA Processing Plants (IGAM) [4], approximately six million tons of IBA is generated annually. Despite this substantial volume, progress toward the utilization of IBA remains underdeveloped. The same report indicates that about 10% of the total IBA is processed in metal recycling, while less than 20% is reused in construction sectors.

This limited utilization is concerning because IBA contains valuable materials and thus can be considered an alternative substitute for natural resources. In this context, approximately 85% of its composition comprises essential minerals in addition to metal fractions, including critical and precious metals in high demand. Furthermore, this underutilization of IBA is particularly concerning because of the growing tendency of MSW production in Germany [5]. Further development is even more demanding, driven by the increasing pressure on landfill capacity, the environmental risks associated with long-term waste disposal, and the growing awareness of sustainable resource management. Consequently, repurposing IBA has gained significant attention in recent years; thus, developing feasible and scalable processes to valorize it has become an urgent priority.

Despite its potential as an alternative secondary material, the challenge in utilizing IBA lies in efficiently separating metallic and mineral components to maximize the recovery of valuable materials while minimizing impurities. Various methods have been explored for this purpose, including mechanical processing and physical separation techniques. Among these, a sequence of magnetic, eddy current, and density-based separations has become a standard industrial practice in Germany and Europe for isolating metal-rich constituents from mineral fractions [6,7]. Despite all these efforts and depending on official regulations, this mineral fraction, also known as processed IBA (pr.IBA), still has limited utilization in expected applications in the construction sector.

As is also the case in the boundary of German regulation, the primary identified challenge in utilizing pr.IBA in construction sectors remains associated with chemical barriers, as once reported by Verbinnen et al. [8]. This challenge involves the presence of undesired metals like aluminum, the leaching of heavy metals such as copper, and the presence of salts containing chloride. Nonetheless, based on several comprehensive reviews regarding the treatment process of IBA [9–11], introducing an extended operation to pr.IBA involving further comminution (increasing the degree of liberation) followed by additional separation (refining the yielded product) to separate the metal-bearing fraction from the mineral fraction has been relatively overlooked. In this context, only one report is accessible from van de Wouw et al. [12], who proposed a perspective on the applicability of crushing using a jaw crusher, followed by state-of-the-art separation techniques to enhance IBA beneficiation. Considering this unexplored possibility of further beneficiations employing the comminution process as a supplement to the current recovery operation of IBA, this research aims to provide an additional perspective on extended material recovery from pr.IBA. Since the applicability of selective milling has been explored in another dedicated report [13], this study focuses on the material separation process from selectively milled pr.IBA in providing alternative materials for both metal recycling (ferrous and non-ferrous) and mineral recovery for the construction sector.

2. Experimental Results

2.1. Observations on the Products of Magnetic and Eddy Current Separations

The average chemical compositions of the first products after the magnetic (MF/CF 010-Mag) and eddy current (MF/CF 010-NE and MF/CF 010-Min) separation of MF010 and CF010 are provided in Tables 1 and 2, respectively. Based on these analysis results, enrichments in certain elements are observable, particularly in CF010. Predictably, the highest iron content was detected in MF/CF 010-Mag, and the highest aluminum content coupled with copper (including Zn, Pb, and Sn) was measured in MF/CF 010-NE.

Table 1. Average chemical composition (XRF) of separation products from MF010.

Elements (wt.%)	Major Comp. of MF010- -Mag	-NE	-Min	Elements (ppm)	Minor Comp. of MF010- -Mag	-NE	-Min
Si	22.7	34.3	30.1	Sr	387	218	304
Ca	12.2	6.7	10.2	Zr	336	240	263
Fe	11.6	0.7	1.5	Ni	401	62	93
Al	3.9	4.3	2.7	Sn	134	159	112
Na	2.3	3.7	2.6	Sb	173	73	87
Mg	1.4	0.8	1.0	Co	92	40	40
Ti	0.81	0.29	0.60	Mo	60	9	19
K	0.87	0.63	0.88	V	60	17	27
S	0.70	0.26	0.50	Rb	30	20	34
Cu	0.26	0.65	0.20	Nb	20	7	12
Zn	0.39	0.23	0.33	As	9	22	9
Cl	0.44	0.15	0.35				
P	0.40	0.13	0.29				
Ba	0.28	0.14	0.20				
Mn	0.18	0.04	0.07				
Pb	0.07	0.11	0.09				
Cr	0.11	0.02	0.03				

Note: The share of MF010-Mag, -NE, and -Min is 58%, 5%, and 37%, respectively. Furthermore, the composition averages three measurement results per batch across three batches.

Table 2. Average chemical composition (XRF) of separation products from CF010.

Elements (wt.%)	Major Comp. of CF010- -Mag	-NE	-Min	Elements (ppm)	Minor Comp. of CF010- -Mag	-NE	-Min
Si	20.7	20.8	30.3	Sr	401	193	362
Ca	12.7	7.5	10.3	Zr	324	318	479
Fe	16.9	1.2	2.3	Ni	452	178	333
Al	3.8	21.5	2.6	Sn	199	990	267
Na	2.5	2.8	3.6	Sb	140	128	84
Mg	1.5	0.9	1.1	Co	83	13	52
Ti	0.79	0.28	0.47	Mo	55	20	24
K	0.63	0.64	0.74	V	64	38	30
S	0.53	0.68	0.34	Rb	24	33	31
Cu	0.70	7.37	0.47	Nb	25	10	16
Zn	0.35	1.73	0.36	As	7	22	16
Cl	0.28	0.29	0.23				
P	0.32	0.16	0.22				
Ba	0.29	0.13	0.18				
Mn	0.25	0.12	0.12				
Pb	0.07	1.03	0.20				
Cr	0.13	0.03	0.18				

Note: The share of CF010-Mag, -NE, and -Min is 51%, 5%, and 44%, respectively. Furthermore, the composition averages three measurement results per batch across three batches.

Complementary to the as-received analysis, the dominance of the silicon concentration is detected in all separation products of MF010 and CF010. These observations are subsequently supported by the XRD analysis of MF/CF 010-Mag and MF/CF 010-Min (graphs are provided in the Appendices A and B), where silicate-bearing phases are predominantly detected, which include quartz (SiO_2), wollastonite ($CaSiO_3$), akermanite ($Ca_2MgSi_2O_7$), diopside ($CaMgSi_2O_6$), and different olivine groups (M_2SiO_4—M: Ca, Fe, Mn, Ni, Mg, etc.). Furthermore, given that these silicate phases also contain calcium at specific contents, a similar distribution of calcium can also be observed in all products except MF/CF 010-NE, which is presumably related to the compositional constraint effect, given the notably high concentration of non-ferrous elements (particularly Al and Cu).

The enrichment of aluminum- and copper-based alloys in metallic form is also elucidated in Figures 1b and 2b for MF010-NE and CF010-NE, respectively. The figures indicate that well-distributed bright particles (potentially Al-based in white and Cu-based in orange and yellow) are contained in the output non-ferrous, coupled with some other residual substances, including silicates. Interestingly, the counts of these non-ferrous metals also support the fact that the concentrations of both Al and Cu in the CF010-NE sample are higher than those in the MF010-NE sample, as listed in Tables 1 and 2. By comparing the contrast in the output non-ferrous with the output mineral, some residual non-ferrous particles can still be detected, as documented in Figures 1c and 2c for MF010-Min and CF010-Min, respectively. In this instance, the count of copper is relatively noticeable, particularly in the coarse fraction, which is a portion of almost 5000 ppm according to the chemical analysis results in Table 2. Intriguingly, considering different input materials listed in Table 3, this Cu content in the output mineral might not necessarily be constant but floating at specific ranges, as provided by the XRF analysis results in Table 4, which is also indicating that further separation might be necessary depending on the demanded requirements of the expected future application.

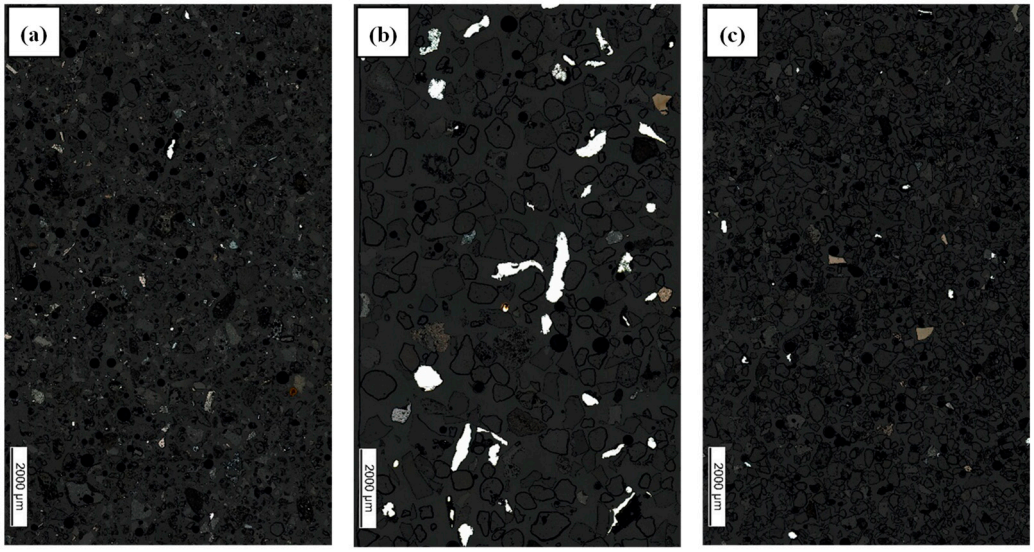

Figure 1. Metallography (stitching) of (**a**) MF010-Mag, (**b**) MF010-NE, and (**c**) MF010-Min.

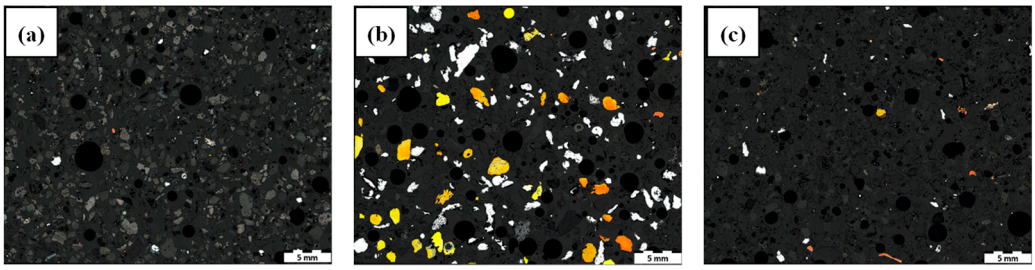

Figure 2. Metallography (stitching) of (**a**) CF010-Mag, (**b**) CF010-NE, and (**c**) CF010-Min.

A similar case also applies to the magnetic fraction, especially CF010-Mag, as documented in Figure 2a. Despite indicating a relatively lower count of copper particles, its copper content is higher than that of CF010-Min, reaching a value of around 7000 ppm. This pattern can also be seen for the different sources of pr.IBA listed in the XRF analysis results in Tables 4 and 5. In this case, a different form of copper should be expected, which might correlate with distinct iron-based substances. This argument is based on the fact that despite the high iron content listed in Tables 1 and 2, bright particles representing the anticipated existence of iron metal are barely observable both in Figures 1a and 2a for MF010-Mag

and CF010-Mag, respectively. Supported by the XRD results in the Appendix A, the magnetic fractions are dominated by iron oxides, especially magnetite, with additional minor indications of hematite, fayalite, and wustite components.

Table 3. Average chemical compositions (wt.%) of selective milling products MF and CF from various pr.IBAs sourced from different IBA processing plants.

Products	Si	Ca	Fe	Al	Cu	Zn	Mn	Cr
MF010	26.0	11.4	6.9	3.7	0.27	0.38	0.14	0.09
MF1032	24.6	9.8	5.9	4.3	0.16	0.22	0.12	0.06
MF010var.Af	27.9	9.6	2.1	3.5	0.17	0.22	0.07	0.04
MF010var.Bf	26.5	9.5	2.7	4.6	0.19	0.37	0.09	0.04
CF010	24.6	11.0	11.0	4.6	0.80	0.47	0.25	0.10
CF1032	22.8	10.0	11.8	5.6	0.60	0.23	0.17	0.15
CF010var.Af	27.9	9.0	2.4	3.7	0.27	0.22	0.08	0.05
CF010var.Bf	27.0	8.8	2.0	5.1	0.27	0.44	0.09	0.04

Note: The chemical composition is the average value from more than five selective milling trials for each pr.IBA sourced from different IBA processing plants.

Table 4. Average chemical compositions (wt.%) of output mineral: classified fraction of selective milling products MF and CF from various pr.IBAs sourced from different IBA processing plants.

Products	Si	Ca	Fe	Al	Cu	Zn	Mn	Cr
MF010-Min	30.1	10.2	1.5	2.7	0.20	0.33	0.07	0.03
MF1032-Min	29.1	9.8	1.3	3.6	0.18	0.46	0.07	0.04
MF010var.Af-Min	28.9	8.2	1.1	2.5	0.09	0.13	0.05	0.03
MF010var.Bf-Min	29.9	8.1	1.1	2.8	0.19	0.27	0.04	0.02
CF010-Min	30.3	10.3	2.3	2.6	0.47	0.36	0.12	0.18
CF1032-Min	29.5	8.8	1.6	3.5	0.36	0.47	0.10	0.22
CF010var.Af-Min	28.9	7.5	0.9	2.3	0.06	0.11	0.05	0.04
CF010var.Bf-Min	28.1	7.9	1.1	3.5	0.12	0.20	0.03	0.03

Note: The chemical composition averages three measurements per batch across three batches of separation for various pr.IBAs sourced from different IBA processing plants.

Table 5. Average chemical compositions (wt.%) of magnetic fraction: classified fraction of selective milling products MF and CF from various pr.IBAs sourced from different IBA processing plants.

Products	Si	Ca	Fe	Al	Cu	Zn	Mn	Cr
MF010-Mag	22.7	12.2	11.6	3.9	0.26	0.39	0.18	0.11
MF1032-Mag	22.4	15.4	8.9	4.8	0.23	0.66	0.25	0.22
MF010var.Af-Mag	26.1	10.7	3.6	4.3	0.13	0.25	0.13	0.05
MF010var.Bf-Mag	21.4	11.4	7.8	5.0	0.25	0.24	0.12	0.05
CF010-Mag	20.7	12.7	16.9	3.8	0.70	0.35	0.25	0.13
CF1032-Mag	22.0	13.5	12.2	4.7	0.22	0.51	0.24	0.24
CF010var.Af-Mag	20.4	12.0	7.6	5.8	0.17	0.35	0.24	0.09
CF010var.Bf-Mag	20.6	12.3	5.7	6.8	0.23	0.33	0.26	0.07

Note: The chemical composition averages three measurements per batch across three batches of separation for various pr.IBAs sourced from different IBA processing plants.

It is contextually correct to declare that the magnetic fraction at this point possesses the highest iron content in the middle and coarse fractions despite fluctuations, corresponding to the input materials in Table 3. However, such an iron content is relatively low compared to what is offered to iron and steel producers, who typically prefer an iron content of around 60 wt.%, around the composition of lump iron ore [14–16]. Therefore, an additional magnetic separation process was conducted to enrich the iron concentrate, as presented in Table 6, for both MF/CF 010 and MF/CF 1032.

Table 6. Average chemical composition (wt.%) of outputs high- and low-magnetic in MF and CF from magnetic fractions of 0–10 mm and 10–32 mm pr.IBAs in Table 5.

Products	Si	Ca	Fe	Al	Cu	Zn	Mn	Cr
MF010-HFe	8.1	8.9	40.1	2.0	0.25	0.50	0.47	0.40
MF1032-HFe	9.0	10.1	36.8	2.3	0.31	0.55	0.46	0.38
CF010-HFe	7.7	7.0	42.1	1.9	0.89	0.36	0.36	0.27
CF1032-HFe	9.9	9.3	37.5	2.1	0.31	0.44	0.44	0.34
MF010-LFe	23.5	13.0	6.1	3.6	0.22	0.32	0.12	0.06
MF1032-LFe	24.3	16.1	5.0	5.2	0.21	0.67	0.23	0.12
CF010-LFe	21.4	13.6	10.2	3.9	0.58	0.31	0.19	0.09
CF1032-LFe	24.3	14.4	7.0	5.2	0.21	0.52	0.21	0.13

Note: The chemical composition averages three measurements per batch across three batches of separation for 0–10 mm and 10–32 mm pr.IBAs.

Increasing the iron content mentioned earlier could be an alternative for valuably utilizing iron-containing outputs. However, application in iron and steel production is not the only prospective option. The analysis results in Table 6 confirmed that all the output high-magnetic (-HFe) still possessed relatively unchanged copper contents, indicating that copper was somehow attached to the high-magnetic fraction. Depending on the quality of the steel that would be manufactured and the copper concentration in the output high-magnetic that would be charged into the process, the level of copper as a common impurity in some steel grades [17,18] would immediately become the next challenge. Consequently, considering the mass fraction of the output high-magnetic documented in Table 7, which is relatively insignificant (just above the output non-ferrous yet with anticipated lower market prices), shifting the valorization perspective to copper recovery should be more promising instead. Therefore, the forthcoming sections assess the second alternative regarding copper concentration.

Table 7. Mass balance of fractions and outputs relative to 0–10 mm and 10–32 mm pr.IBAs.

Fractions/Outputs		MF010-	CF010-	MF1032-	CF1032-
-Mag		26.6%	14.5%	31.7%	18.2%
	-HFe	3.7%	2.6%	3.9%	3.2%
	-LFe	22.9%	11.9%	27.8%	15.0%
-NMag		19.5%	13.6%	15.4%	11.9%
	-NE	2.4%	1.3%	0.7%	0.7%
	-Min	17.1%	12.3%	14.7%	11.2%

2.2. Observations on the Products of Density Separation

As mentioned earlier and complementary to the Materials and Methods Section, the density separation process was conducted in a laboratory-scale apparatus. Moreover, this process only considered three specific outputs from the prior separation sequences. Specifically, the studied samples comprise three particular outputs that contain notable copper concentration, CF010-LFe, CF010-NE, and CF010-Min, which follow distinguishable contexts and aims of copper recovery:

1. CF010-LFe was selected to demonstrate the recovery potential of copper content from the magnetic fraction as the second option in addition to iron recovery.
2. CF010-NE was selected as the next possible alternative for utilizing this output in the copper recycling industry, where aluminum is not commonly desired.
3. CF010-Min was selected to explore the possibility of further enhancing its cleanliness from heavy metals, including lowering the copper concentration.

Since the classification using an air-table density separator is used to physically separate materials based on their weight differences, a relatively (nearly) uniform particle size must be guaranteed for optimal classification. Therefore, a sieving operation was initially performed, and only fractions between 0.5 and 2.0 mm were considered in this section because of the technical limitations of the air-table density separator employed during this experiment, which is why only the CF was involved. However, the selection of this particle size range does not reduce the applicability and reliability of the density separation approach since the selected range already accounts for a significant fraction of the total mass, and the modification of the air-table density separator is still obviously possible. Accordingly, five different sieve classes were utilized, and the chemical compositions of only the heaviest and lightest fractions after density separation are listed in Table 8 as a representation of the complete dataset provided in the Appendix C.

Table 8. Chemical composition of heaviest and lightest fractions of five different particle size distributions covering particle size between 0.5 and 2.0 mm of CF010-LFe.

Particle Size (mm)	Density ($g.cm^{-3}$)	Elements in Fractions (wt.%—XRF Method)							
		Si	Ca	Fe	Al	Cu	Zn	Mn	Cr
0.50–0.71	3.33	13.0	11.5	28.3	3.3	0.52	0.53	0.53	0.39
0.71–1.00	3.62	10.5	8.9	36.1	2.5	0.83	0.60	0.58	0.45
1.00–1.18	4.09	7.5	6.0	44.9	1.9	0.89	0.42	0.73	0.38
1.18–1.40	4.22	7.1	5.8	45.7	1.5	1.52	0.37	0.70	0.24
1.40–2.00	5.07	4.1	3.3	49.9	1.5	3.70	0.64	1.11	0.73
0.50–0.71	2.27	23.7	14.9	5.6	6.8	0.20	0.48	0.18	0.09
0.71–1.00	2.51	24.4	14.1	6.3	6.0	0.19	0.42	0.20	0.11
1.00–1.18	2.47	24.5	12.8	5.9	7.1	0.23	0.39	0.18	0.10
1.18–1.40	2.62	25.2	13.5	5.9	6.0	0.21	0.41	0.19	0.10
1.40–2.00	2.27	24.9	12.7	5.2	7.9	0.18	0.39	0.19	0.11

Note: The chemical composition averages three measurements per batch across two batches of separation. The approach also applies to Tables A1–A5 in Appendix C.

The results presented in Table 8 and the complete dataset in the Appendix C demonstrate that density separation effectively concentrates copper content. Furthermore, the data indicate that larger particle sizes correspond to higher copper concentrations in the heaviest fraction. This trend in copper enrichment is corroborated by the metallography analysis shown in Figure 3, which highlights the presence of typical yellow and orange copper particles. Similarly, iron content exhibits a positive correlation with this copper enrichment trend. In contrast, the silicon, calcium, and aluminum concentrations show an inverse relationship, decreasing with increasing density. A similar method was also applied to the output non-ferrous (CF010-NE), yet only heavy and light fractions were produced. Unlike CF010-LFe, which focuses on element concentration trends, CF010-NE aims to isolate copper-bearing particles for recycling. As a result, the product representation of heavy fractions from CF010-NE is documented in Figure 4.

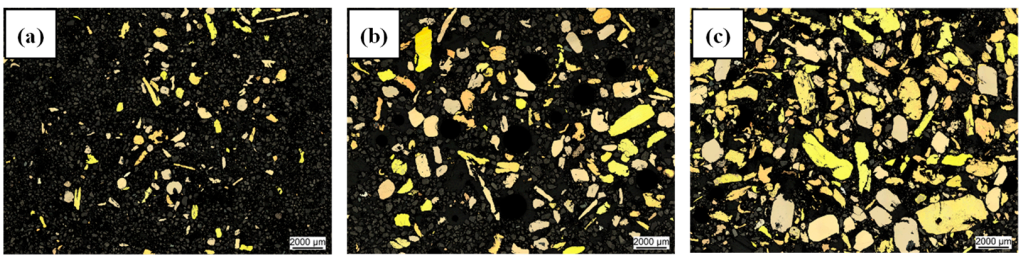

Figure 3. Metallography (stitching) of heaviest fraction from CF010-LFe after density separation at different particle classifications: (**a**) 0.50–0.71 mm, (**b**) 1.00–1.18 mm, and (**c**) 1.40–2.00 mm.

Figure 4. Heavy fractions from CF010-NE after density separation at different particle classifications: (**a**) 0.50–0.71 mm, (**b**) 1.00–1.18 mm, and (**c**) 1.40–2.00 mm.

A typical representation of non-ferrous particles manifested in yellow and orange colors under a light microscope representing copper-bearing particles is also shown in Figure 5. Based on this EDS analysis, the composition of mixed-sample heavy fractions from CF010-NE after density separation is substantiated by elemental mapping, which revealed that copper-based alloys dominated the products. Specifically, a high contrast of Cu (orange) was recorded with indications of Zn (cyan) and Sn (red), which are the two most common alloying elements of copper-based alloys (brass and bronze). In addition, some oxide phases are also captured, either attached to copper-bearing particles or some residual materials from the separation.

In contrast, a greater number of possible non-metallic compounds are captured in the light fraction of CF010-NE after the density separation process. This fraction is rationally foreseen since it possesses a density of approximately 2.6 g/cm^3 (compared with the heavy fraction of up to 6.1 g/cm^3), which is comparable to the density of aluminum and various minerals. This argument is further elucidated in Figure 6, where the results of a metallography analysis conducted are shown. This analysis shows that only white-bright particles are observable in the light fraction, indicating a possible metallic phase in a predominantly non-metallic population. Furthermore, the EDS elemental mapping results reveal that the metallic particles are aluminum-based metals (blue) surrounded by various non-metallic substances (in the case of Figure 6, they could be sulfide, oxide, or sulfate) that are either attached to or entirely separated from aluminum.

In addition to separating CF010-LFe and CF010-NE, a similar density separation process was also applied to CF010-Min. Despite having a relatively low level of copper, as indicated in Tables 2 and 4, a certain level of recovery can still be attained. It is important to note that the density separation process for the output mineral primarily aims to remove heavy metals (not only copper) or heavy-metal-bearing particles, which is considered critical before further application in the construction sector. Specifically, clean and stable materials are necessary for an expected application as a substitute for natural aggregates in concrete because no additional process is foreseen.

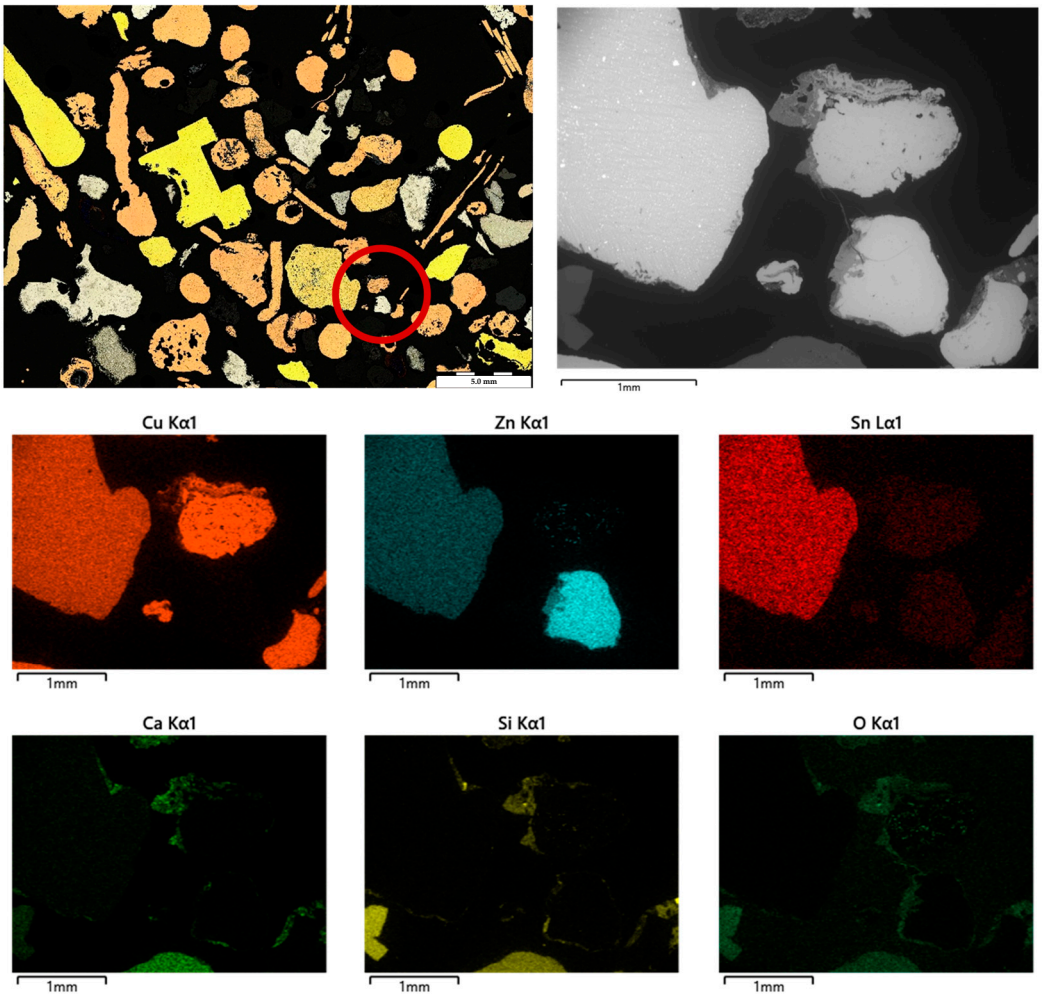

Figure 5. Elemental mapping (EDS) from a mixed sample of heavy fractions from CF010-NE. The EDS mapping represents the particles in the red circle.

In this context, in contrast to CF010-LFe, only two sieve classes were considered due to the circumstances of CF010-Min. It is correlated with the characteristic of CF010-Min as an output mineral, which is already clean and predominated by mineral substances, where a vast amount of material will be required to produce an adequate amount of the heavy fraction to conduct a proper analysis. Therefore, the two largest classes were selected in this laboratory trial, and their heavy fractions are provided in Figure 7.

Based on the metallography analysis in Figure 7, relatively fewer copper-bearing particles are captured than in the two previous results for the heaviest fractions in CF010-LFe and CF010-NE. This disparity is still correlated with the previously mentioned circumstances that lead to the heaviest fraction of CF010-Min possessing a density of just up to 3 g/cm^3. However, the process is relatively effective since the XRF analysis indicates that the reduction potential of the copper content in the lightest fraction can reach a value lower than 1000 ppm, as listed in Table 9. Therefore, the determining factor during large-scale implementation is a balance between the cost of separation, total usable material volume, and standard quality requirements.

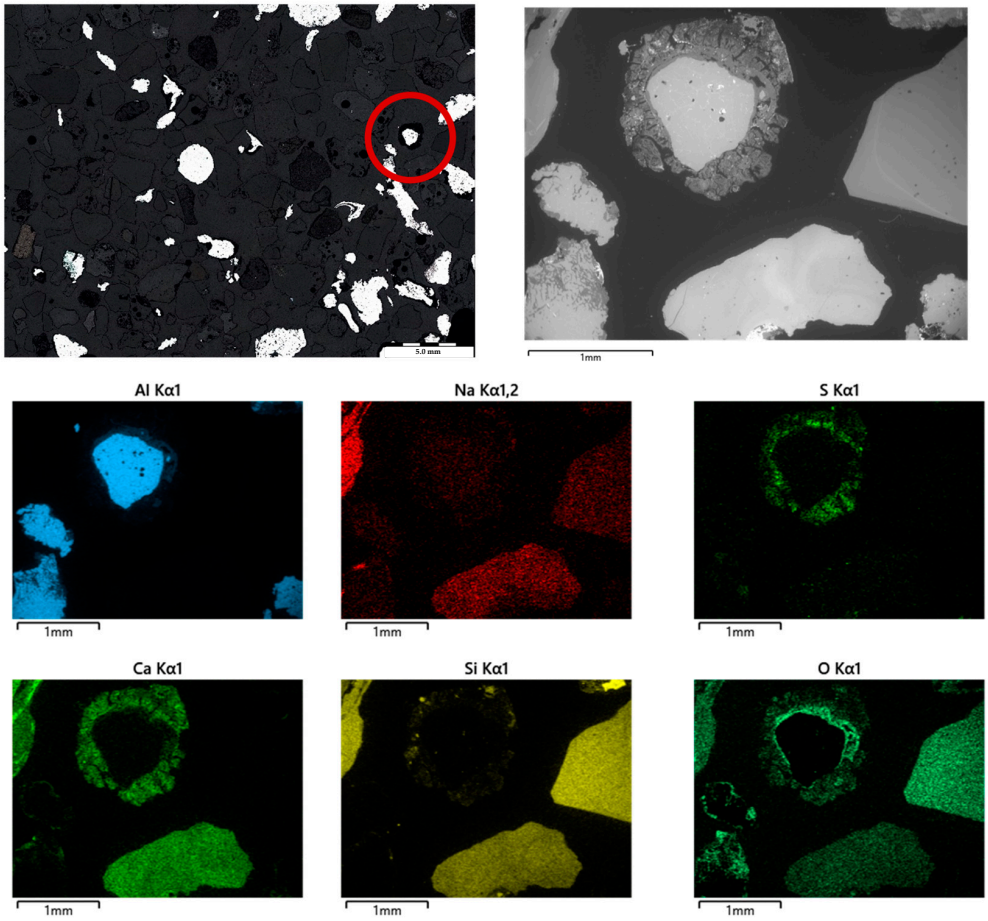

Figure 6. Elemental mapping (EDS) from a mixed sample of light fractions from CF010-NE. The EDS mapping represents the particles in the red circle.

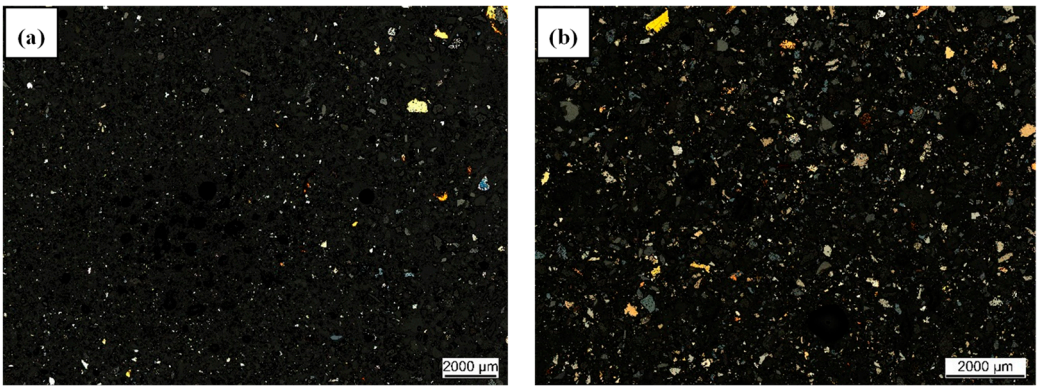

Figure 7. Metallography (stitching) of heaviest fraction from CF010-Min after density separation at different particle classifications: (**a**) 1.18–1.40 mm and (**b**) 1.40–2.00 mm.

Table 9. Chemical composition of lightest fractions from two different particle size distributions covering particle size between 1.18 and 2.0 mm of CF010-Min.

Particle Size (mm)	Elements in Fractions (wt.%—XRF Method)							
	Si	Ca	Fe	Al	Cu	Zn	Mn	Cr
1.18–1.40	32.9	10.2	1.5	4.6	0.09	0.17	0.08	0.04
1.40–2.00	34.0	9.8	1.4	3.6	0.08	0.16	0.07	0.04

Note: The chemical composition averages three measurements per batch across two batches of the density separation process.

3. Materials and Methods

3.1. pr.IBA as the Primary Origin of the Investigated Sample

The investigated sample in this study originated from processed IBA (designated further as pr.IBA), which represents only a certain fraction of the original raw IBA. Specifically, pr.IBA is generated as a residual material from state-of-the-art recovery processes to raw IBA, involving a set of screening, magnetic, and eddy current separation processes typically performed by IBA processing companies in Germany. As detailed in Figure 8, raw IBA refers to fresh and wet bottom ash produced from MSWI, with an annual production volume of approximately 6 million tons. This raw IBA underwent natural weathering for two to three months before being further processed, involving a series of screening and separation sequences in bottom ash processing facilities.

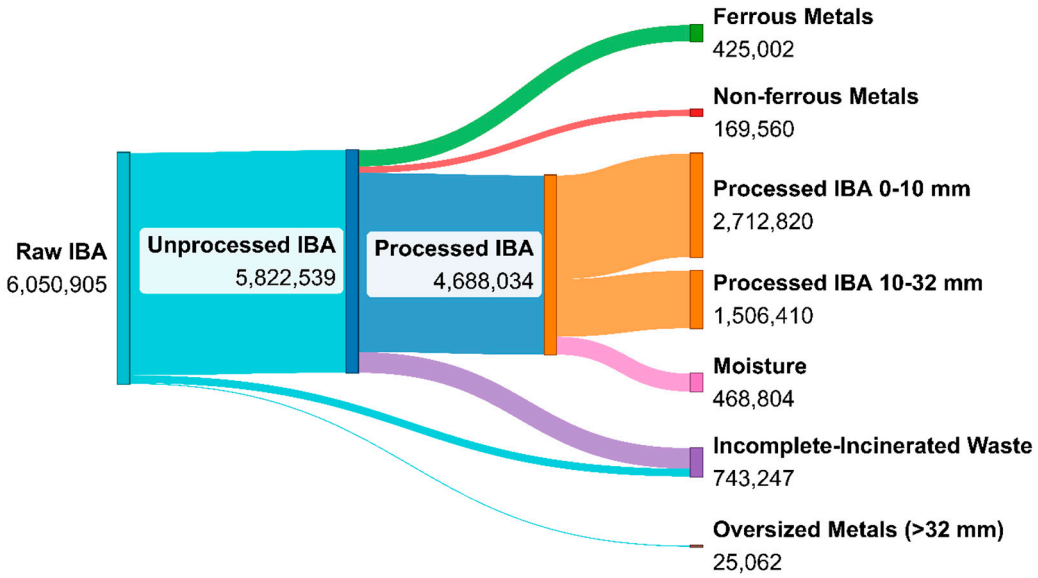

Figure 8. The theoretical annual mass balance (tons) of IBA in Germany [4,19].

The process begins with classification, where oversized metals (>32 mm) are removed as scrap for recycling, while incompletely incinerated waste is returned to the incineration process. This procedure leaves an unprocessed IBA residual fraction, which serves as the input material for subsequent separation operations, with an expected annual volume of around 5.9 million tons in Germany. The following classification of bottom ash processing plants involves a combination of sieving, magnetic, and eddy current separation processes. This sequence produces three distinct fractions, ferrous metals, non-ferrous metals, and pr.IBA, as presented in Figure 8. In this case, pr.IBA can be subdivided into two particle size ranges, 0–10 mm and 10–32 mm, with estimated volumes of 2.7 million tons and 1.5 million tons, respectively.

3.2. The Selective Milling Process as a Pre-Concentration Step for pr.IBA

In addition to the typically performed processing sequence provided in Figure 8, 0–10 mm and 10–32 mm samples of pr.IBA (each sample weight of around three tons sourced from an IBA processing plant in the western part of Germany) were selectively milled to produce three different products. Selective milling was performed using a vertical milling machine operated by LOESCHE in their test center in Neuss, Germany. Details about the procedure and applicability of this approach as a concentration step in enhancing the valorization opportunity of pr.IBA are provided in a dedicated report [13]. As mentioned, three different milling products are yielded: fine fraction (FF), middle fraction (MF), and coarse fraction (CF) with primary particle sizes of <200 µm, 0.2–0.5 mm,

and >0.5 mm, respectively. In this case, extending the mass balance in Figure 8 in addition to the proportion of these products, the average annual prospective material volume in the boundary of selective milling considered in a previous study is represented in Figure 9.

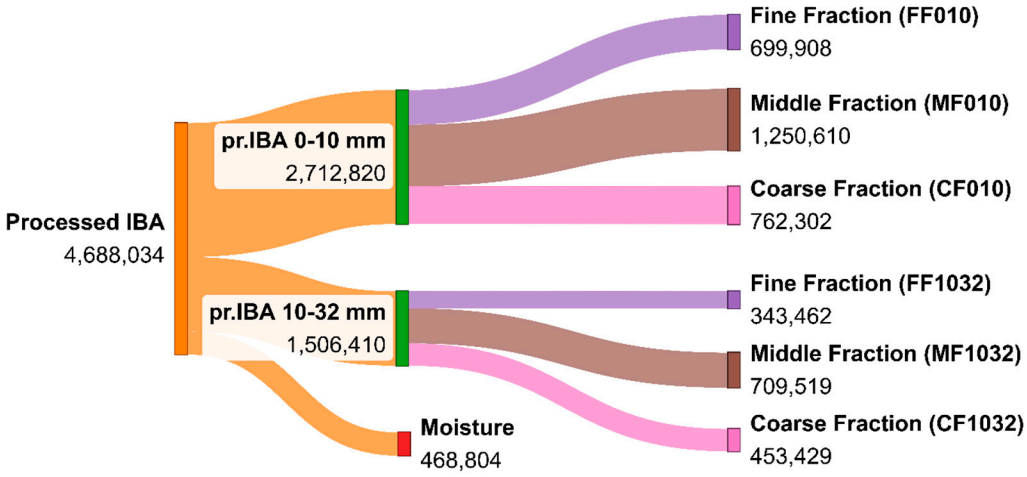

Figure 9. The average theoretical annual mass (tons) of pr.IBA in Germany after milling [13].

Conclusively, as provided in Figure 9 and considering the further expected applications (the fine fraction is intended to be used in cement clinker production), only the middle fraction (MF010) and coarse fraction (CF010) were considered the primary investigated samples in this study. In addition, similar separation sequences were also used to refine the middle and coarse fractions from selective-milled 10–32 mm pr.IBA and two additional 0–10 mm pr.IBAs (var.Af and var.Bf), sourced from an IBA processing plant in the northern part of Germany (as also explored in [13]). These supplementary trials were carried out to compare product qualities in the case of variation in the input materials.

3.3. Magnetic, Eddy Current, and Density Separations

Compared with the average composition of as-received 0–10 mm pr.IBA (AR), the initial chemical compositions of the primary investigated samples (MF010 and CF010) in this study are provided in Table 10. Approximately 100 kg of each sample (three batches) was separated using a magnetic and eddy current separation sequence, and some products were additionally concentrated using density separation. Specifically, the process was started using a high-intensity rapid magnetic separator belt to remove all magnetic materials from the stream, yielding magnetic (MF/CF 010-Mag) and non-magnetic fractions (MF/CF 010-NMag). Afterward, the magnetic fraction was refined using a low-intensity magnetic drum to produce output high-magnetic (MF/CF 010-HFe) and output low-magnetic (MF/CF 010-LFe). On the other hand, the non-magnetic fraction was separated by employing an eddy current separator, yielding two additional products: output non-ferrous (MF/CF 010-NE) and output mineral (MF/CF 010-Min).

Both magnetic and eddy current separations were conducted in a demonstration-scale separator from STEINERT in Pulheim, Germany. In this instance, the trials for MF010 and CF010 were conducted separately to ensure separation effectiveness during the process and to analyze the products carefully regarding chemical composition. Furthermore, dry density separation, which complements the magnetic and eddy current separation sequence, was subsequently performed. This method proved to be a reliable classification process, as reported in [20–22]. Nonetheless, this technique focused only on copper recovery from three outputs due to its copper content and particle size: CF010-LFe, CF010-NE, and CF010-Min. Additionally, since the density separation process was conducted in laboratory facilities in Duisburg, Germany, only around 10 kg per batch of these products was considered (two

trial batches of each product). The process was started by sieving the input material into different particle classifications (ranging from 0.5 to 2.0 mm) before classifying it into several density classes using an air-table density separator supplied by TRENNSO-TECHNIK from Weißenhorn, Germany.

Table 10. The initial chemical composition (XRF) of the as-received 0–10 mm pr.IBA (AR) and its milling products as the primary investigated samples: MF010 and CF010.

Elements	Major Components			Elements	Minor Components		
(wt.%)	AR	MF010	CF010	(ppm)	AR	MF010	CF010
Si	22.5	25.6–27.2	23.4–26.4	Sr	390	339–371	306–574
Ca	13.9	10.7–11.8	10.2–12.0	Zr	343	305–329	262–464
Fe	7.7	6.4–7.6	8.4–14.1	Ni	292	279–314	219–517
Al	3.9	3.6–3.8	3.5–5.9	Sn	235	129–152	128–586
Na	2.4	1.9–2.7	3.0–3.4	Sb	174	139–149	117–244
Mg	1.3	1.1–1.2	1.3–1.6	Co	75	75–88	65–116
Ti	0.76	0.68–0.72	0.59–0.70	Mo	45	43–48	35–72
K	0.83	0.80–0.94	0.54–0.73	V	43	38–46	33–45
S	1.04	0.51–0.82	0.41–0.65	Rb	35	29–35	23–31
Cu	0.56	0.26–0.29	0.38–1.27	Nb	16	14–18	14–35
Zn	0.54	0.35–0.41	0.31–0.71	As	11	2–19	3–18
Cl	0.55	0.34–0.50	0.22–0.36				
P	0.33	0.32–0.38	0.22–0.31				
Ba	0.26	0.24–0.25	0.22–0.33				
Mn	0.15	0.13–0.14	0.13–0.85				
Pb	0.14	0.08–0.09	0.08–0.61				
Cr	0.08	0.08–0.09	0 08–0.16				

Note: The AR values are an average of five different measurement results on a stockpile of 0–10 mm pr.IBA. Moreover, the MF010 and CF010 data are the min-max values of more than five selective milling trials for 0–10 mm pr.IBA.

In terms of chemical analysis, the main products generated from magnetic and eddy current separations were comprehensively analyzed using X-ray fluorescence (XRF) coupled with X-ray diffraction (XRD) methods. Furthermore, a set of metallography analyses employing a light microscope and scanning electron microscopy with energy-dispersive X-ray spectroscopy (SEM/EDS) was also carried out, especially for metal-rich outputs. In the light microscope case, a stitching approach was performed to provide an overview of the whole sample instead of looking at one coincidental observation area. Stitching means that several metallography images are digitally combined to construct a broader perspective on the observed sample. Finally, for the results from density separation, a Gay-Lussac pycnometer was used to approximate the density of each fraction.

4. Material Recovery After Extended Separation of Selectively Milled pr.IBA

Based on the results of the present study, it is once again substantiated that IBA holds immense and promising potential as a reliable alternative secondary resource for both the metal and mineral industries. This similar potential remains even for pr.IBA. Despite undergoing sophisticated separation processes using state-of-the-art classification techniques, an additional valuable product stream can still be promisingly generated from pr.IBA once extended operations are carried out, as elucidated in this study. Considering the specific case in Germany where a total mass of six million tons of raw IBA is produced annually, as shown in Figure 8, a new potential mass and product stream following the selective milling process shown in Figure 9 and extended material classifications for both

0–10 mm and 10–32 mm pr.IBAs at the boundary of the present study are provided in Figures 10 and 11, respectively.

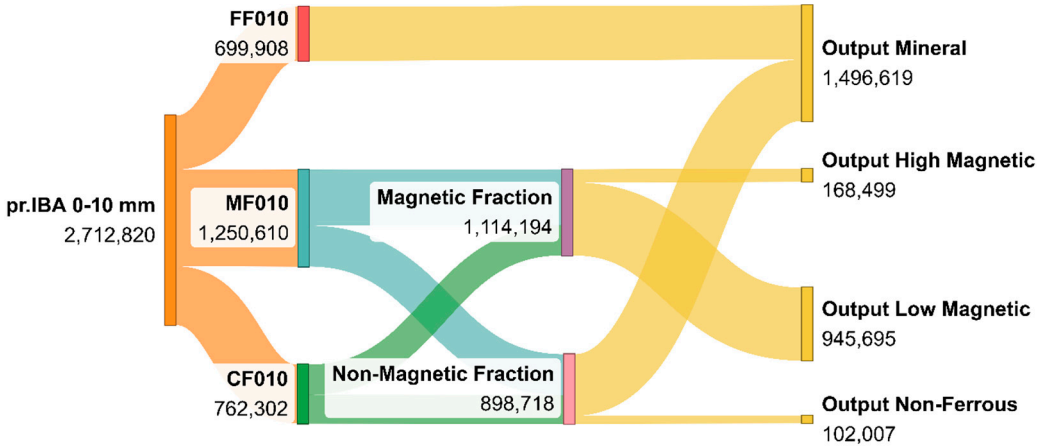

Figure 10. The expected annual mass (tons) separation output of 0–10 mm pr.IBA in Germany.

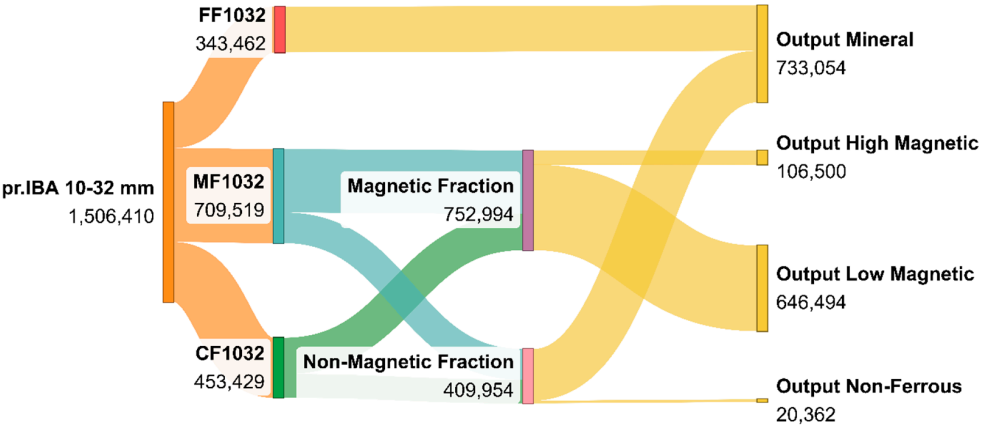

Figure 11. The expected annual mass (tons) separation output of 10–32 mm pr.IBA in Germany.

Based on the Sankey diagram provided in Figures 10 and 11, four primary outputs can be generated from the extended process proposed in the present research, including an output mineral, output high-magnetic, output low-magnetic, and output non-ferrous, which are coded in the previous sections following the designations of -Min, -HFe, -LFe, and -NE, respectively. In the case of the output mineral, including the fine fraction (one direct product from selective milling), a total annual material volume of 2.2 million tons is theoretically foreseen. Considering its characteristics, this output holds the potential to be used in the construction sector, including clinker and concrete production (positive implementations are provided in dedicated reports [19]).

This argument is based on the chemical composition results in Table 4, which show that there is a significant reduction in heavy metal concentration, yet this is associated with silicon enrichment and a notable calcium content. Taking MF-Min into account, by enriching these two elements in its composition, this output offers a substitute for primary charge materials for the raw mix in clinker production. Specifically, instead of employing natural SiO_2 and $CaCO_3$ in clinker production, charging a portion of MF-Min into the process could be worthwhile. Supported by the XRD analysis results, the silicon and calcium contents available in MF-Min are expected to form silicate-based materials, thus offering additional advantages for reducing CO_2 emission due to the reduction in the amount of $CaCO_3$ used as input materials upon substitution with MF-Min as well as the fine fraction (FF). Despite this promising potential, it is still worth mentioning that

MF-Min is barely equivalent to a natural source in terms of impurities. Thus, dedicated examinations are necessary because certain foreign substances can affect cement quality, as comprehensively reported by Kolovos et al. [23,24]. Nonetheless, the effect is known to be proportional to the charged concentration compared with the raw mix, as substantiated by different researchers documented in [25,26], which is practicable considering the amount of available MF-Min and FF compared with the total cement clinker production in Germany, which reaches a volume of nearly 25 million tons annually [27].

The last fraction of the discussed output mineral is the contribution from CF-Min. Based on the initial analysis provided in Tables 3 and 10, the chemical composition of the coarse fraction was relatively more contaminated than that of the middle fraction. This gap is related to the selective milling results in [13], where the coarse fraction is observed to be a segregation point for the heavy metals in pr.IBA. However, after conducting magnetic and eddy current separation processes, a significant reduction in metal content was recorded in Table 2, which is much more notable than the result for the middle fraction in Table 1. However, because of its current composition and particle size distribution, the use of CF-Min as a substitute for natural aggregates in concrete rather than clinker production is more promising.

Consequently, compared with its utilization in clinker production for FF and MF-Min, the challenge in using CF-Min as an alternative aggregate material in concrete production is that no additional processing or considerable chemical reactions can be expected. Hence, CF-Min should be physically and chemically stable. Considering the origin of CF-Min and the chemical analysis results in Table 4, this study also demonstrated that a refined separation process is still practicable. One possible option is employing density separation to CF-Min, where a certain degree of separation can be achieved. Table 9 reports that this process generates a potentially cleaner mineral constituent coupled with the concentrated metal-bearing fraction captured in Figure 7. However, as mentioned in the previous section, such an additional separation sequence should match the practical balance between the material volume, quality requirements, and resulting cost. Therefore, a dedicated examination of the employment of CF-Min in concrete production before deciding on any additional processes is essential. One of the substantial issues is deciding whether further metal separation is necessary, or it is more critical to remove chloride (as suggested by Verbinnen et al. [8]) and glass particles instead. As documented in Figure 12, a glass phase is captured and can transform into a challenge at a specific content limit regarding the alkali–silica reaction in concrete, as reported in [28–30].

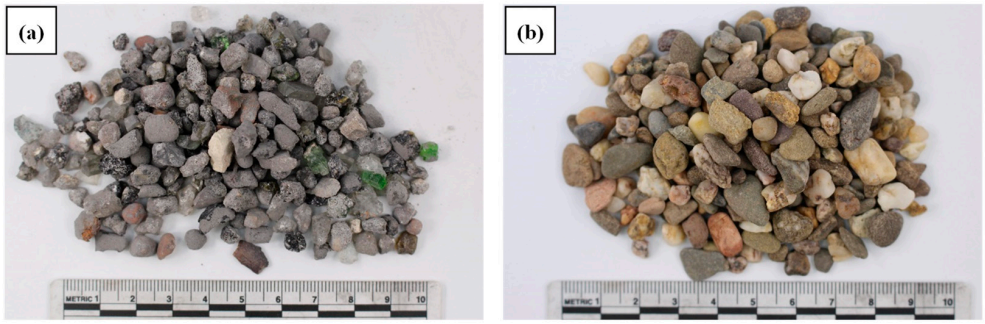

Figure 12. A visual comparison between (**a**) CF010-Min and (**b**) a typical natural aggregate for concrete production—the representation only shows the particle size range of 4.0–8.0 mm.

The product generated from this extended separation sequence in this study is the magnetic fraction, which theoretically accounts for a total mass of almost 1.9 million tons in Germany yearly. As shown in Tables 1 and 2, the highest iron content can be measured in this magnetic fraction. However, as shown in Table 5, the measured iron content is too low

(<20 wt.% Fe) compared with the iron ore grade practically charged in the blast furnace process for efficient iron production. Therefore, a complementary concentration step, which includes additional magnetic separation and density separation, was considered in the present study. As documented in Tables 6 and 8, both methods successfully increased the iron content to approximately 40 wt.% Fe, which is more useful than 20 wt.% Fe for iron production. This is supported by Zhong et al. [31], who conducted a set of trials using a feed with 34 wt.% Fe. Their results indicated that competitive iron recovery could be attained, thus opening an opportunity for conducting recycling practices using secondary materials. However, to ultimately compete with conventional iron ore, such an iron-bearing material might require more effort in the beneficiation process before entering the market [32], which is currently volatile due to the transformation in the iron industry. In this instance, adjusting the parameters for magnetic and density separations is still possible before eventually arriving at an economical limit.

These ideas were not entirely novel in providing an alternative method for valorizing low-grade iron ore. From the view of density separation, Chaurasia and Nikkam [33] suggested that a multi-gravity separation method could be a reliable beneficiation process for low-grade iron ore. However, this method highly depends on the mineralogical characteristics of the input material. Wang et al. [34] reported that iron recovery from low-grade ore is more challenging if its mineralogical characteristics are excessively complex, which is the general case for IBA. Alternatively, developed magnetic separation methods were suggested by various researchers in [35,36] by using relatively similar iron contents, as listed in Tables 6 and 8. However, the central question regarding profitability remains the determining factor, given that the generated final products are an insignificant part of the theoretical amount of 0.3 million tons of output high-magnetic and 1.6 million tons of output low-magnetic.

Considering a profitable approach to valorizing the magnetic fraction, shifting the aim to recovering copper could be more useful given its higher market price than iron. The analysis results in Tables 1 and 2 indicate that, in addition to copper, notable valuable metal enrichment in the magnetic fraction is also recorded. The enriched elements include Mn, Cr, Ni, Sb, Co, and Mo, which are related to the iron content in terms of alloying elements bound together in a silicate matrix or associated with a spinel structure, as reported by Wei et al. [37]. The latter is more probable since less metallic iron (bright particles under a light microscope) was captured, as shown in Figures 1a and 2a. In this instance, the present study substantiated that a copper concentrate could be generated from the magnetic fraction using the density separation technique. As shown in Table 8 and Figure 3, in addition to the complete analysis in the Appendix C, it is elucidated that copper can reliably be recovered. Interestingly, some heavy metals were also collected with the copper concentrate in the heavy fraction listed in Table 8, which consequently offers an additional clean material stream that can be utilized to supplement the output mineral for clinker and concrete production.

Based on these results, the adjustment of separation parameters should intentionally be aimed at meeting the quality requirements in the construction sector since the residual fraction will possess a high copper content at least comparable to the head grades of copper in exploited ore, as provided by Flores et al. [38]. However, it is worth noting that the beneficiation of the copper-bearing fraction needs more exploration since its form is not equivalent to the copper in natural ore. Compared to typically exploited copper ore, various copper-bearing compounds can be expected in IBA, including a heterogeneous mixture of metallic phase, oxides, and sulfide, as reported by Keber et al. [39]. Furthermore, in the case of residual iron, in contrast to copper as an impurity in iron production, metallic iron in copper production is considered beneficial as a reducing agent. A similar case is

also applicable during clinker production, where a particular iron content is necessary to establish a liquid phase of tetracalcium alumina ferrite.

This approach using density separation in recovering copper has also proven effective in separating copper particles from the output non-ferrous (the copper-richest fraction in this extended separation sequence), with a theoretical annual volume in Germany of more than 0.1 million tons. As documented in Figure 5, the separated copper-containing fraction consists mainly of copper-based alloys, which can be directly charged into the smelting process in the copper production step. Despite being relatively minor compared with other outputs within the boundary of this study, this copper-bearing fraction could be the most revenue-generating product, as reported by Muchova et al. [40]. However, further analysis is still necessary if this is also the case in the present study.

Additionally, the residual fraction containing aluminum (Figure 6) can also be further processed using a relatively simple method that involves only grinding and sieving. Figure 13 shows how grinding the light fraction of CF010-NE could recover the aluminum in Figure 6. The idea is based on the fact that aluminum (and copper) in CF010-NE is ductile enough to prevent pulverization (only flattening) during grinding, unlike the accompanying impurities, which are mainly brittle substances and will rapidly become powder upon the application of a grinding process. In addition, this mechanism is common for pretreatment during the recycling of aluminum dross, as reported in [41,42].

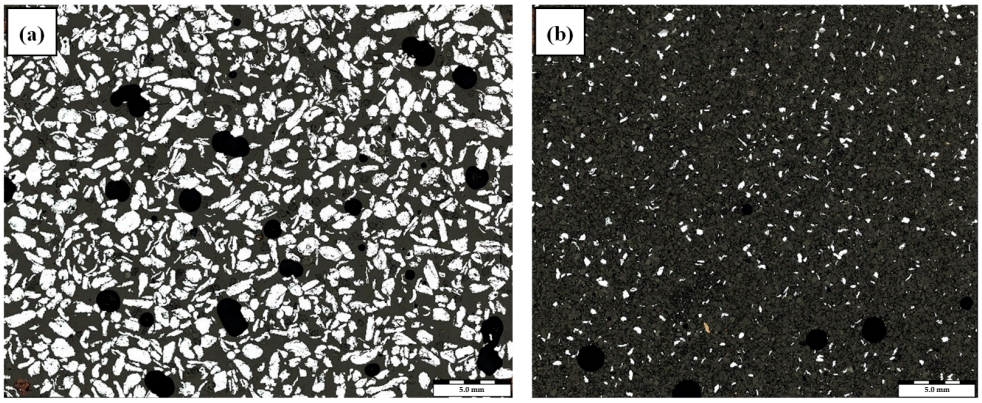

Figure 13. Metallography (stitching) of (**a**) oversized and (**b**) undersized particles after grinding and sieving of light fraction from CF010-NE in Figure 6.

5. Conclusions

Although already undergoing a sequence of separation processes carried out by IBA processing plants, pr.IBA still possesses immense potential associated with its metal and mineral concentrations, which this study demonstrated can be recovered once an extended separation process is carried out. Based on the results of the present study, the following conclusions could be drawn regarding the recovery of materials from pr.IBA after an extended separation process:

1. By integrating supplementary separation after a selective milling process, a precise method was developed for accumulating the most valuable and profit-generating products in pr.IBA, which is a consequence of the effort to obtain a clean mineral substance as a substitute for natural materials in the construction sector.
2. Four valuable outputs or secondary products could be obtained following the extended separation process suggested in the present study: output mineral, output high-magnetic, output low-magnetic, and output non-ferrous.
3. The output mineral comprises the fraction that is relatively liberated from a specific content of heavy metal and thus can be beneficial for cement and concrete

production. Considering the fact that MF-Min, in addition to the FF, is composed of calcium-bearing silicate phases, this fraction could be beneficial in reducing both the consumption of natural materials and carbon emission due to the decreasing necessity of $CaCO_3$.

4. In the case of CF-Min, an additional separation process could still be performed due to its particle size. One alternative would be to conduct density separation to separate the heavy fraction, which is typically associated with heavy metals. However, the balance between material volume, resulting cost, and quality requirements should be initially explored.
5. Despite accumulating the iron-bearing fraction, the Fe content in the magnetic fraction is relatively lower than what is practically offered in the iron and steel industries. In this instance, an additional magnetic or density separation process is proven to be able to enrich the iron concentration to around 40%.
6. As an alternative to iron recovery, a copper separation process from the magnetic fraction could be a more useful alternative driven by its higher market prices. In this case, the copper content is successfully concentrated using the density separation method, resulting in an additional clean fraction for the output mineral.
7. The density separation method was also proven to be applicable to the separation of copper from residual substances from output non-ferrous, which can potentially be charged to the copper smelting process. In addition, the aluminum fraction can also be recovered from the resulting light fraction by using a fine-grinding technique.
8. The extent of the separation process should remain within the scope of its intended application. The goal should be to ensure the method achieves a sufficient separation level without compromising the quality of the final product. This approach allows the cost and energy required for excessive separation to be redirected toward addressing other challenges (e.g., chloride and glass removal).

Author Contributions: I.B.G.S.A.: Conceptualization, Methodology, Validation, Investigation, Formal Analysis, Data Curation, Writing—Original Draft, and Visualization. K.R.: Formal Analysis, Investigation, Data Curation, Writing—Original Draft, and Visualization. K.-H.B.: Methodology, Data Curation, Validation, Formal Analysis, Investigation, and Resources. A.K.: Methodology, Validation, Formal Analysis, Investigation, and Resources. R.W.: Conceptualization. Methodology, Resources, Writing—Review and Editing, Supervision, Project Administration, and Funding Acquisition. R.D.: Conceptualization, Methodology, Validation, Formal Analysis, Resources, Writing—Review and Editing, Supervision, Project Administration, and Funding Acquisition. All authors have read and agreed to the published version of the manuscript.

Funding: This study was supported by the funding program ReMin: Resource Efficient Circular Economy—Construction and Mineral Material Cycles (Project EMSARZEM: FKZ 033R265) under the Research for Sustainable Development Program (FONA) initiated by the Federal Ministry of Education and Research (BMBF), Federal Republic of Germany. The authors also acknowledge support from the Open Access Publication Fund of the University of Duisburg-Essen.

Data Availability Statement: The original contributions presented in this study are included in the article. Further inquiries can be directed to the corresponding authors.

Acknowledgments: The authors acknowledge the support of Winfried Ruhkamp from LOESCHE GmbH for managing the selective milling process, as well as Aneta Knöpfelmacher and Stefan Seemann from VDZ Technology gGmbH and Henning Jansen from DK Recycling und Roheisen GmbH for the thorough chemical analyses, including XRD and XRF.

Conflicts of Interest: I.B.G.S.A., K.R., and R.D. certify they have no conflicts of interest to declare. K-H.-B. and A.K. are employed by the company STEINERT GmbH; R.W. is employed by the company GKS-Gemeinschaftskraftwerk Schweinfurt GmbH. The remaining authors declare that this research

was conducted in the absence of any commercial or financial relationships that could be construed as potential conflicts of interest.

Appendix A. XRD Results of Magnetic Fraction (MF/CF 010-Mag)

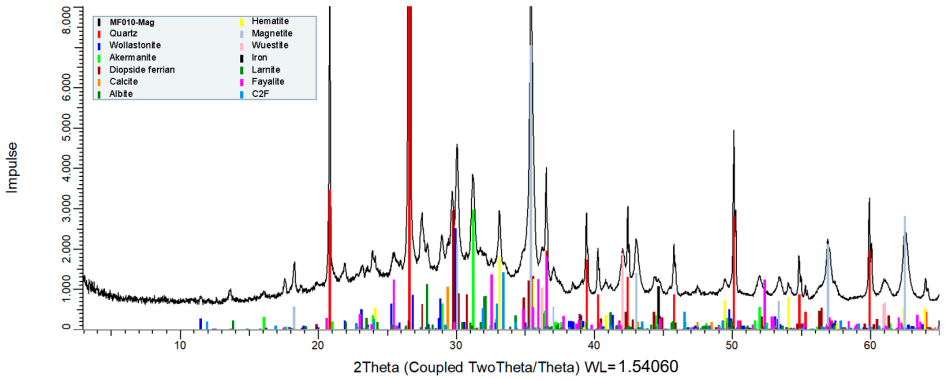

Figure A1. XRD results of MF010-Mag: part of magnetic fraction originated from middle fraction (MF) of selective-milled 0–10 mm pr.IBA after magnetic separation.

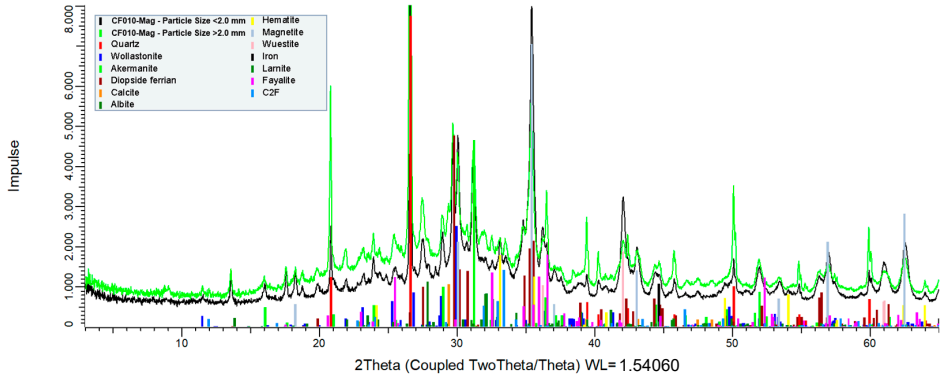

Figure A2. XRD results of CF010-Mag: part of magnetic fraction originated from coarse fraction (CF) of selective-milled 0–10 mm pr.IBA after magnetic separation.

Appendix B. XRD Results of Output Mineral (MF/CF 010-Min)

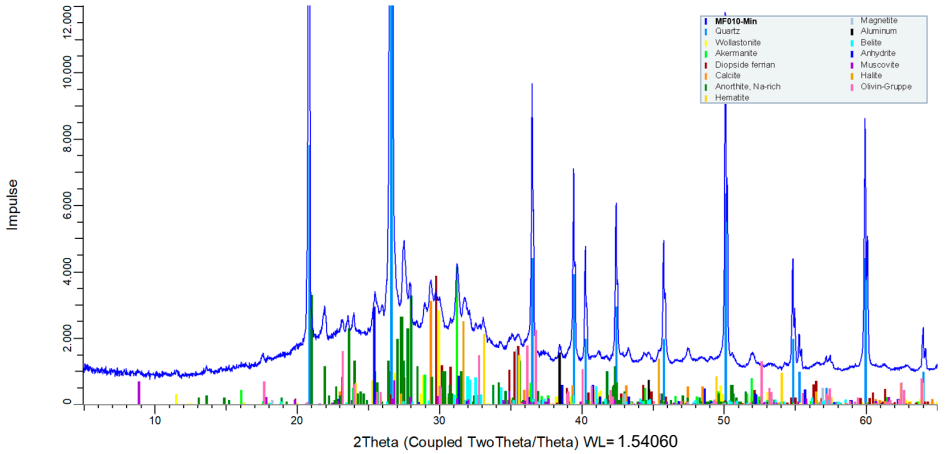

Figure A3. XRD results of MF010-Min: part of output mineral originated from middle fraction (MF) of selective-milled 0–10 mm pr.IBA after magnetic and eddy current separations.

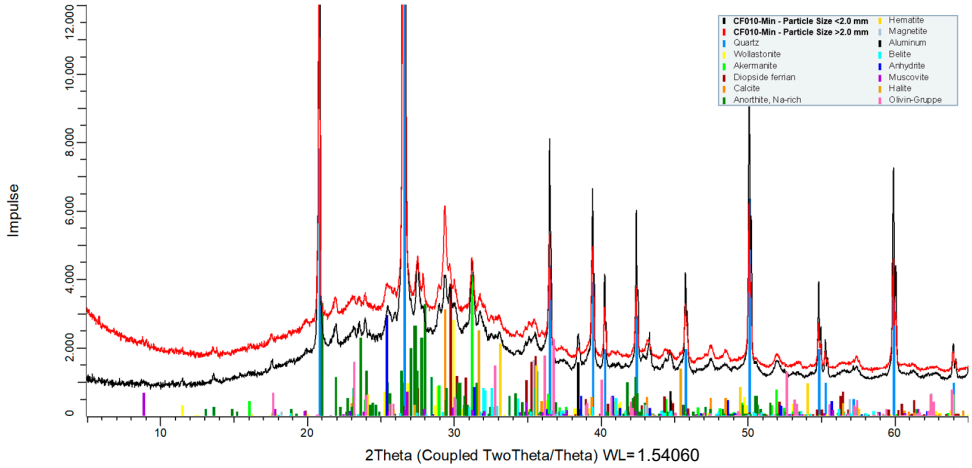

Figure A4. XRDs result of CF010-Min: part of output mineral originated from coarse fraction (CF) of selective-milled 0–10 mm pr.IBA after magnetic and eddy current separations.

Appendix C. XRF Results of Density Separation for CF010-LFe

Table A1. Chemical composition of CF010-LFe particle size 0.50–0.71 mm after density separation.

Mass Fraction (% to CF010-LFe)	Density ($g.cm^{-3}$)	Elements in Fractions (wt.%—XRF Method)							
		Si	Ca	Fe	Al	Cu	Zn	Mn	Cr
2.9%	3.33	13.0	11.5	28.3	3.3	0.52	0.53	0.53	0.39
0.2%	2.78	20.5	15.9	10.8	4.9	0.26	0.46	0.31	0.18
1.3%	2.75	21.2	15.6	10.1	5.1	0.23	0.46	0.29	0.17
2.2%	2.71	23.3	14.8	7.3	5.7	0.22	0.44	0.22	0.13
0.6%	2.27	23.7	14.9	5.6	6.8	0.20	0.48	0.18	0.09

Table A2. Chemical composition of CF010-LFe particle size 0.71–1.00 mm after density separation.

Mass Fraction (% to CF010-LFe)	Density ($g.cm^{-3}$)	Elements in Fractions (wt.%—XRF Method)							
		Si	Ca	Fe	Al	Cu	Zn	Mn	Cr
2.8%	3.62	10.5	8.9	36.1	2.5	0.83	0.60	0.58	0.45
1.3%	3.10	16.6	14.2	19.7	3.7	0.39	0.57	0.44	0.24
1.8%	2.93	19.0	15.5	14.3	4.2	0.35	0.49	0.34	0.18
5.5%	2.77	21.8	15.4	9.7	4.9	0.26	0.45	0.28	0.15
4.4%	2.51	24.4	14.1	6.3	6.0	0.19	0.42	0.20	0.10

Table A3. Chemical composition of CF010-LFe particle size 1.00–1.18 mm after density separation.

Mass Fraction (% to CF010-LFe)	Density ($g.cm^{-3}$)	Elements in Fractions (wt.%—XRF Method)							
		Si	Ca	Fe	Al	Cu	Zn	Mn	Cr
0.8%	4.09	7.5	6.0	44.9	1.9	0.89	0.41	0.73	0.38
2.3%	3.31	15.3	12.8	23.8	3.5	0.42	0.47	0.45	0.22
1.8%	2.99	19.4	15.2	13.6	4.6	0.29	0.53	0.33	0.20
4.2%	2.75	22.8	14.9	8.9	4.9	0.22	0.42	0.23	0.14
2.4%	2.57	25.0	13.7	6.0	5.8	0.20	0.41	0.19	0.11
0.5%	2.47	24.5	12.8	5.9	7.1	0.23	0.39	0.18	0.10

Table A4. Chemical composition of CF010-LFe particle size 1.18–1.40 mm after density separation.

Mass Fraction (% to CF010-LFe)	Density ($g.cm^{-3}$)	Elements in Fractions (wt.%—XRF Method)							
		Si	Ca	Fe	Al	Cu	Zn	Mn	Cr
0.5%	4.22	7.1	5.8	45.7	1.5	1.52	0.37	0.70	0.24
2.3%	3.42	14.5	12.3	26.1	3.2	0.29	0.53	0.45	0.20
1.2%	3.10	19.3	15.0	14.3	4.1	0.59	0.48	0.33	0.21
3.6%	2.86	22.5	14.8	9.2	5.3	0.31	0.42	0.23	0.15
0.9%	2.70	25.0	13.9	6.3	5.6	0.24	0.41	0.20	0.10
2.6%	2.62	25.1	13.5	5.9	6.0	0.21	0.40	0.19	0.10

Table A5. Chemical composition of CF010-LFe particle size 1.40–2.00 mm after density separation.

Mass Fraction (% to CF010-LFe)	Density ($g.cm^{-3}$)	Elements in Fractions (wt.%—XRF Method)							
		Si	Ca	Fe	Al	Cu	Zn	Mn	Cr
0.3%	5.07	4.1	3.3	49.9	1.2	3.70	0.64	1.11	0.73
3.9%	3.68	11.4	9.3	35.0	2.3	0.94	0.40	0.52	0.19
2.6%	3.27	16.9	13.7	20.2	3.7	0.47	0.45	0.39	0.20
7.7%	3.02	20.4	14.7	13.0	4.5	0.36	0.44	0.28	0.16
10.9%	2.74	24.3	13.9	7.1	5.8	0.26	0.39	0.19	0.12
2.4%	2.27	24.9	12.7	5.2	7.9	0.18	0.39	0.19	0.11

References

1. Rajendran, N.; Gurunathan, B.; Han, J.; Krishna, S.; Ananth, A.; Venugopal, K.; Priyanka, R.B.S. Recent Advances in Valorization of Organic Municipal Waste into Energy using Biorefinery Approach, Environment and Economic Analysis. *Bioresour. Technol.* **2021**, *337*, 125498. [CrossRef] [PubMed]
2. Ghumra, D.P.; Rathi, O.; Mule, T.A.; Khadye, V.S.; Chavan, A.; Barba, F.C.; Main, S.; Odaneth, A.; Thorat, B.N. Technologies for Valorization of Municipal Solid Wastes. *Biofuels Bioprod. Biorefining* **2022**, *16*, 877–890. [CrossRef]
3. Khaire, K.C.; Mehariya, S.; Kumar, B. Valorization of Municipal Solid Wastes in Circular Economy. *Waste Manag. Circ. Econ.* **2024**, *1*, 35–53. [CrossRef]
4. ITAD IGAM. *Umfrage—Aufbereitung von HMV-Schlacken*; Interessengemeinschaft der Thermischen Abfallbehandlungsanlagen in Deutschland e.V.; Interessengemeinschaft der Aufbereiter und Verwerter von Müllverbrennungsschlacken: Berlin, Germany, 2022.
5. Flamme, S.; Hanewinkel, J.; Quicker, P.; Weber, K. *Energieerzeugung aus Abfällen: Stand und Potenziale in Deutschland bis 2030*; Texte 51/2018; Umweltbundesamt: Dessau-Roßlau, Germany, 2018.
6. Bunge, R. Recovery of Metals from Waste Incinerator Bottom Ash. In *Removal, Treatment and Utilisation of Waste Incineration Bottom Ash*; Thomé-Kozmiensky Verlag: Neuruppin, Germany, 2015; pp. 63–143.
7. Holm, O.; Simon, F.-G. Innovative Treatment Trains of Bottom Ash (BA) from Municipal Solid Waste Incineration (MSWI) in Germany. *Waste Manag.* **2017**, *59*, 229–236. [CrossRef]
8. Verbinnen, B.; Billen, P.; Caneghem, J.V.; Vandecasteele, C. Recycling of MSWI Bottom Ash: A Review of Chemical Barriers, Engineering Applications and Treatment Technologies. *Waste Biomass Valorization* **2017**, *8*, 1453–1466. [CrossRef]
9. Dou, X.; Ren, F.; Nguyen, M.Q.; Ahamed, A.; Yin, K.; Chan, W.P.; Chang, V.W.-C. Review of MSWI Bottom Ash Utilization from Perspective of Collective Characterization, Treatment and Existing Application. *Renew. Sustain. Energy Rev.* **2017**, *79*, 24–38. [CrossRef]
10. Šyc, M.; Simon, F.G.; Hykš, J.; Braga, R.; Biganzoli, L.; Costa, G.; Funari, V.; Grosso, M. Metal Recovery from Incineration Bottom Ash: State-of-the-art and Recent Developments. *J. Hazard. Mater.* **2020**, *393*, 122433. [CrossRef] [PubMed]
11. Chen, B.; Perumal, P.; Illikainen, M.; Ye, G. A Review on the Utilization of Municipal Solid Waste Incineration (MSWI) Bottom Ash as a Mineral Resource for Construction Materials. *J. Build. Eng.* **2023**, *71*, 106386. [CrossRef]
12. van de Wouw, P.M.F.; Loginova, E.; Florea, M.V.A.; Brouwers, H.J.H. Compositional Modelling and Crushing Behavior of MSWI Bottom Ash Material Classes. *Waste Manag.* **2020**, *101*, 268–282. [CrossRef] [PubMed]
13. Adhiwiguna, I.B.G.S.; Sahbudin, S.H.; Ruhkamp, W.; Warnecke, R.; Deike, R. Effect of Selective Milling on the Concentration Process of Critical Raw Materials from MSW Incinerator Bottom Ash. *Minerals* **2024**, *14*, 1174. [CrossRef]
14. Wu, S.-L.; Xu, H.-F.; Tian, Y.-Q. Evaluation of Lump Ores for Use in Modern Blast Furnaces as Part of Mixed Burden Practice. *Ironmak. Steelmak.* **2009**, *36*, 19–23. [CrossRef]
15. Harvey, L.D.D. From Iron Ore to Crude Steel: Mass Flows Associated with Lump, Pellet, Sinter and Scrap Iron Inputs. *ISIJ Int.* **2020**, *60*, 1159–1171. [CrossRef]

16. Zhu, D.; Jiang, Y.; Pan, J.; Yang, C. Study of Mineralogy and Metallurgical Properties of Lump Ores. *Metals* **2022**, *12*, 1805. [CrossRef]
17. Daehn, K.E.; Serrenho, A.C.; Allwood, J.M. How Will Copper Contamination Constrain Future Global Steel Recycling? *Environ. Sci. Technol.* **2017**, *51*, 6599–6606. [CrossRef]
18. Jin, H.; Mishra, B. Minimization of Copper Contamination in Steel Scrap. In *Energy Technology 2020: Recycling, Carbon Dioxide Management, and Other Technologies*; Springer: Cham, Switzerland, 2020; pp. 357–364. [CrossRef]
19. Deike, R.; Adhiwiguna, I.; Ruhkamp, W.; Warnecke, R. Einsatz von Rostasche-Feinfraktion < 10 mm als Rohstoff für die Herstellung von Zement und Beton. In *Mineralische Nebenprodukte und Abfälle 11*; Thomé-Kozmiensky Verlag GmbH: Neuruppin, Germany, 2024; pp. 192–209.
20. Holm, O.; Wollik, E.; Bley, T.J. Recovery of Copper from Small Grain Size Fractions of Municipal Solid Waste Incineration Bottom Ash by Means of Density Separation. *Int. J. Sustain. Eng.* **2018**, *11*, 250–260. [CrossRef]
21. Back, S.; Ueda, K.; Sakanakura, H. Determination of Metal-abundant High-density Particles in Municipal Solid Waste Incineration Bottom Ash by a Series of Processes: Sieving, Magnetic Separation, Air Table Sorting, and Milling. *Waste Manag.* **2020**, *112*, 11–19. [CrossRef]
22. Back, S.; Sakanakura, H. Distribution of Recoverable Metal Resources and Harmful Elements depending on Particle Size and Density in Municipal Solid Waste Incineration Bottom Ash from Dry Discharge System. *Waste Manag.* **2021**, *126*, 652–663. [CrossRef] [PubMed]
23. Kolovos, K.; Loutsi, P.; Tsivilis, S.; Kakali, G. The Effect of Foreign Ions on the Reactivity of the CaO-SiO_2-Al_2O_3-Fe_2O_3 System Part I. Anions. *Cem. Concr. Res.* **2001**, *31*, 425–429. [CrossRef]
24. Kolovos, K.; Tsivilis, S.; Kakali, G. The Effect of Foreign Ions on the Reactivity of the CaO-SiO_2-Al_2O_3-Fe_2O_3 System Part II: Cations. *Cem. Concr. Res.* **2002**, *32*, 463–469. [CrossRef]
25. Pan, J.R.; Huang, C.; Kuo, J.-J.; Lin, S.-H. Recycling MSWI Bottom and Fly Ash as Raw Materials for Portland Cement. *Waste Manag.* **2008**, *28*, 1113–1118. [CrossRef]
26. Lam, C.H.K.; Barford, J.P.; McKay, G. Utilization of Incineration Waste Ash Residues in Portland Cement Clinker. *Chem. Eng. Trans.* **2010**, *21*, 757–762. [CrossRef]
27. VDZ. Umweltdaten der Deutschen Zementindustrie 2023. 2024. Available online: www.vdz-online.de/wissensportal/publikationen/umweltdaten-der-deutschen-zementindustrie-2023 (accessed on 20 October 2024).
28. Lam, C.S.; Poon, C.S.; Chan, D. Enhancing the Performance of Pre-cast Concrete Blocks by Incorporating Waste Glass—ASR Consideration. *Cem. Concr. Compos.* **2007**, *29*, 616–625. [CrossRef]
29. Rashad, A.M. Recycled Waste Glass as Fine Aggregate Replacement in Cementitious Materials based on Portland Cement. *Constr. Build. Mater.* **2014**, *72*, 340–357. [CrossRef]
30. Paul, S.C.; Savija, B.; Babafemi, A.J. A Comprehensive Review on Mechanical and Durability Properties of Cement-based Materials Containing Waste Recycled Glass. *J. Clean. Prod.* **2018**, *198*, 891–906. [CrossRef]
31. Zhong, R.; Yi, L.; Huang, Z.; Cai, W.; Jiang, X. Highly Efficient Beneficiation of Low-Grade Iron Ore via Ore–Coal Composite-Fed Rotary Kiln Reduction: Pilot-Scale Study. *JOM* **2020**, *72*, 1680–1686. [CrossRef]
32. Ge, S.; Widajat, E.; Sachdeva, T.; Chomyn, K.; Walker, C.; Cameron, I. A Low-Carbon-Emission Flowsheet for BF-Grade Iron Ore using Advanced Electric Smelting Furnace. In Proceedings of the AISTech 2023—The Iron & Steel Technology Conference and Exposition, Detroit, MI, USA, 8–11 May 2023.
33. Chaurasia, R.C.; Nikkam, S. Beneficiation of Low-grade Iron Ore Fines by Multi-gravity Separator using Optimization Studies. *Part. Sci. Technol.* **2016**, *35*, 45–53. [CrossRef]
34. Wang, T.-x.; Zhu, Y.-m.; Gui, X.-h. Flotation of a New Chelate Collector on Fine Refractory Iron Ore-containing Carbonate. *J. Cent. South Univ.* **2016**, *23*, 1058–1065. [CrossRef]
35. Yu, J.; Han, Y.; Li, Y.; Gao, P.; Sun, Y. Separation and Recovery of Iron from a Low-grade Carbonate-bearing Iron Ore using Magnetizing Roasting followed by Magnetic Separation. *Sep. Sci. Technol.* **2017**, *52*, 1768–1774. [CrossRef]
36. Yuan, S.; Xiao, H.; Wang, R.; Li, Y.; Gao, P. Improved Iron Recovery from Low-grade Iron Ore by Efficient Suspension Magnetization Roasting and Magnetic Separation. *Miner. Eng.* **2022**, *186*, 107761. [CrossRef]
37. Wei, Y.; Shimaoka, T.; Saffarzadeh, A.; Takahashi, F. Mineralogical Characterization of Municipal Solid Waste Incineration Bottom Ash with an Emphasis on Heavy Metal-bearing Phases. *J. Hazard. Mater.* **2011**, *187*, 534–543. [CrossRef] [PubMed]
38. Flores, G.A.; Risopatron, C.; Pease, J. Processing of Complex Materials in the Copper Industry: Challenges and Opportunities Ahead. *JOM* **2020**, *72*, 3447–3461. [CrossRef] [PubMed]
39. Keber, S.; Schirmer, T.; Elwert, T.; Goldmann, D. Characterization of Fine Fractions from the Processing of Municipal Solid Waste Incinerator Bottom Ashes for the Potential Recovery of Valuable Metals. *Minerals* **2020**, *10*, 838. [CrossRef]
40. Muchova, L.; Bakker, E.; Rem, P. Precious Metals in Municipal Solid Waste Incineration Bottom Ash. *Water Air Soil Pollut. Focus* **2008**, *9*, 107–116. [CrossRef]

41. Kudyba, A.; Akhtar, S.; Johansen, I.; Safarian, J. Aluminum Recovery from White Aluminum Dross by a Mechanically Activated Phase Separation and Remelting Process. *JOM* **2021**, *73*, 2625–2634. [CrossRef]
42. Srivastava, A.; Meshram, A. On Trending Technologies of Aluminium Dross Recycling: A Review. *Process Saf. Environ. Prot.* **2023**, *171*, 38–54. [CrossRef]